



Contents lists available at ScienceDirect

Arabian Journal of Chemistry

journal homepage: www.ksu.edu.sa

Potential inhibition of SARS-CoV-2 infection and its mutation with the novel geldanamycin analogue: Ignaciomycin

Antony Stalin^{a,1,*}, Pachaiyappan Saravana Kumar^{b,1}, Balakrishnan Senthamarai Kannan^c, Rajamanikam Saravanan^d, Savarimuthu Ignacimuthu^{b,*}, Quan Zou^{a,*}

^a Institute of Fundamental and Frontier Sciences, University of Electronic Science and Technology of China, Chengdu, 610054 China

^b Xavier Research Foundation, St. Xavier's College, Affiliated to Manonmaniam Sundaranar University, Palayamkottai – 627002, Tamil Nadu, India

^c Department of Chemistry, Tirunelveli Dakshinamara Nadar Sangam (T D M N S) College, Valliyur, Tirunelveli 627113, Tamil Nadu, India

^d Department of Physics, Meenakshi Chandrasekaran College of arts and science, Karambayam, Pattukkottai, Thanjavur, 614626

ARTICLE INFO

Keywords:

SARS-CoV-2
Mutations
Ignaciomycin
Molecular docking
Dynamics simulation
Viral inhibitor

ABSTRACT

The impact of novel coronavirus (SARS-CoV-2) is very high; its mutant variants provide a higher transmission rate. Due to many mutations in the omicron-variant, it can evade previously available neutralizing antibodies. The inhibitory effect of the novel compound "Ignaciomycin" was investigated using various computational analyses against the RBD of the SARS-CoV-2 wild-type, Delta, and omicron-variants. Molecular docking revealed the potentially stable interaction of Ignaciomycin with an energy value of -8.65 kcal/mol for the omicron-variant. DFT and Hirshfeld surface calculations showed higher efficiency and reactivity with strong electrostatic potential values. *In-silico* toxicity studies revealed a significant drug-likeness score (7.5912) with non-toxic properties. MD simulation studies confirmed the stability of Ignaciomycin during ~ 100 ns simulation. Covariance, PCA, and FEL analyses revealed significant fluctuations in residues and atom mobility in all variants based on the strong interaction of Ignaciomycin. Mutations in the Delta and omicron-variants increased the binding efficiency of the RBD of the SARS-CoV-2 S-glycoprotein with human ACE2. Ignaciomycin had high efficiency in interacting with mutated sites in the RBD, thereby blocking the interaction of the RBD with ACE2. Our findings provide a strong hypothesis for preclinical validation of Ignaciomycin as a potential drug against SARS-CoV-2 and its mutant variants.

1. Introduction

The coronavirus (COVID-19) pandemic caused by SARS-CoV-2 continuously disturbs human health and the world's economic condition. According to the COVID-19 Data Repository developed by Johns Hopkins University (JHU) (Dong et al., 2020), there have been approximately 630 million infected cases and 6 million deaths by 2022. So far, developed vaccines have quietly controlled death rates. However, the virus emerges with various mutations and increased interaction between the human ACE2 receptor, thus evading the neutralizing antibodies (Shang et al., 2020, Yan et al., 2020, Yang et al., 2021, Zhang et al., 2021, Chen et al., 2022, Lupala et al., 2022). The World Health Organization (WHO) continuously monitors all mutant variants and designates some of the essential variants as "variants of concern" (VOC).

Of all mutant variants, Delta (B.1.617.2) and Omicron (B.1.1.529) are the crucial mutants. Omicron is the current VOC strong interaction with the ACE2-receptor based on the mutations in the receptor binding domain (RBD) of the spike (S) glycoprotein, which significantly neutralize antibodies and form strong electrostatic and hydrophobic surfaces in the receptor binding motif (RBM) of the spike protein (Cao et al., 2022a, Cheng et al., 2022). There are more than 30 mutations in Omicron, and about 15 mutations are in the RBD region (Cao et al., 2022b, Ren et al., 2022).

The spike protein is the critical hotspot antigenicity site for many drugs and antibodies. Due to the unprecedented mutations and the need to develop novel antibodies and drugs targeting the emerging mutations and their resistances and consider immune escape (Lupala et al., 2022). The main thing is that SARS-CoV-2 is a respiratory disease that majorly

* Corresponding authors.

E-mail addresses: antonystalin@uestc.edu.cn, a.staanlin@gmail.com (A. Stalin), imuthus@hotmail.com, ignacimuthu@stxavierstn.edu.in (S. Ignacimuthu), zouquan@nclab.net, zouquan@uestc.edu.cn (Q. Zou).

¹ These authors contributed equally to this work.

<https://doi.org/10.1016/j.arabjc.2023.105493>

Received 19 June 2023; Accepted 26 November 2023

Available online 28 November 2023

1878-5352/© 2023 The Author(s). Published by Elsevier B.V. on behalf of King Saud University. This is an open access article under the CC BY-NC-ND license (<http://creativecommons.org/licenses/by-nc-nd/4.0/>).

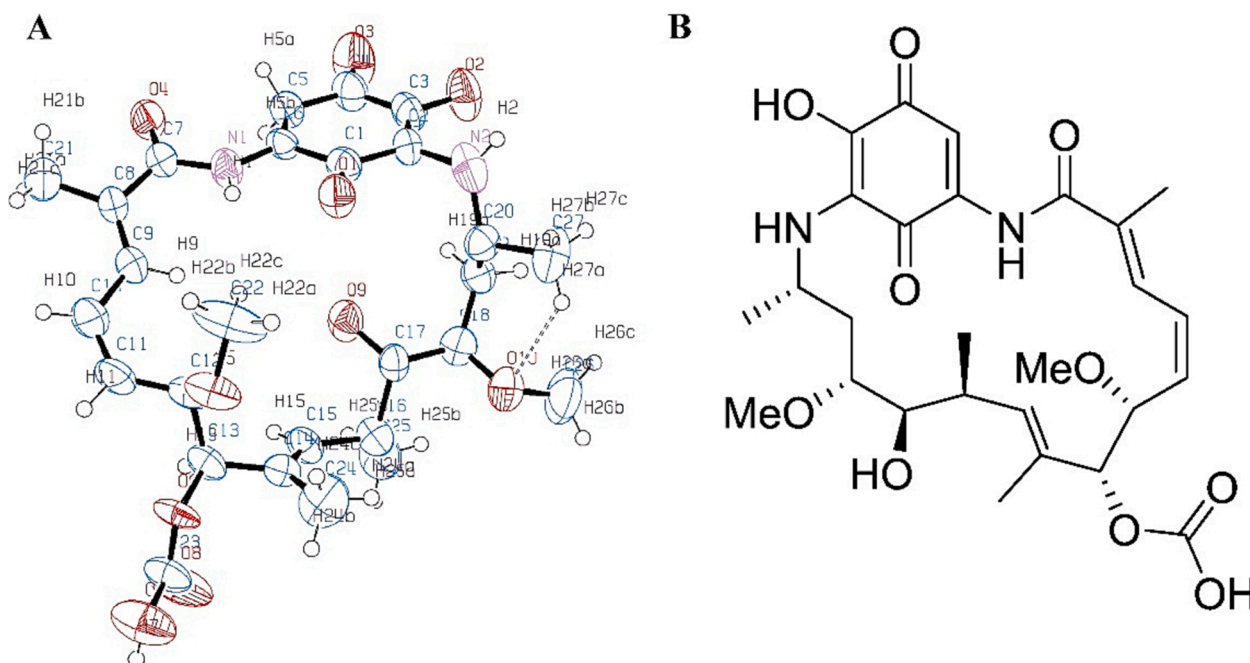


Fig. 1. Structure of Ignaciomyacin. (A) ORTEP diagram of the newly derived Geldanamycin analogue compound Ignaciomyacin. (B) 2D structure of Ignaciomyacin.

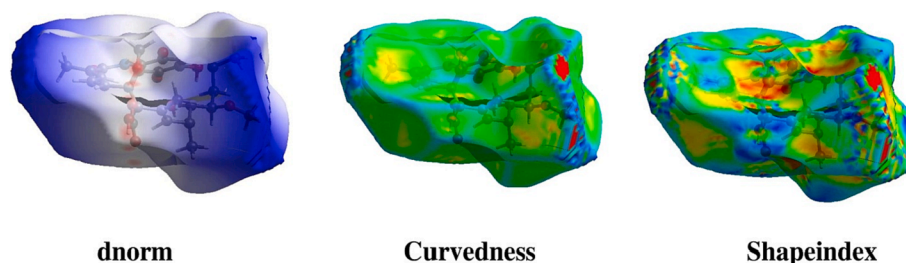


Fig. 2. Physicochemical structural analysis. Hirshfeld diagram over d_{norm} , Curvedness, and Shape index of Ignaciomyacin.

affects the lungs; at the same time, it can also affect other organs because of immune suppression (Arokiyaraj et al., 2020, Bajo-Morales et al., 2022, Jacob et al., 2022). Due to the neutralizing antibody evasion by the omicron variant, there is an urgent need to develop novel drugs with significant activity. Numerous research reports revealed the inhibitory properties of various natural products from plants, fungi, bacteria, and nanoparticle-based vaccines and drugs against bacterial and viral infections, including SARS-CoV-2 (Arokiyaraj et al., 2020, Nikaeeen et al., 2020, Tam et al., 2021, Yousefi et al., 2021a, Yousefi et al., 2021b, Zulfiqar et al., 2021, Akter et al., 2022, Mahdi et al., 2022, Stalin et al., 2022b, Xu et al., 2023).

Geldanamycin belongs to the group of ansamycins, a class of benzoquinones, and is known for its antimicrobial and anticancer activities. However, the use of geldanamycin is restricted due to its hepatotoxicity and other undesirable effects (Taechowisan et al., 2020, Skrzypczak et al., 2021). In addition, geldanamycin is a major inhibitor of heat shock protein 90 (HSP90) and also has antiviral properties against viruses such as influenza and HIV-1. Therefore, geldanamycin analogues and derivatives are continuously being developed to increase its efficacy and reduce side effects (Connor et al., 2007, Li et al., 2012, Sultan et al., 2020).

In the current study, the newly obtained compound “Ignaciomyacin” (an analogue of geldanamycin) from the terrestrial *Streptomyces* sp. CFR16 was investigated for its inhibitory effect against SARS-CoV-2 infection. The RBD of wild-type SARS-CoV-2 S-glycoprotein (<https://www.rcsb.org/structure/6M0J>), Delta (<https://www.rcsb.org/struc>

<https://www.rcsb.org/structure/7V8B>) and Omicron (<https://www.rcsb.org/structure/7T9L>), was chosen for the *in silico* molecular docking analysis, followed by molecular dynamics simulation and covariance matrix with the principal component analysis. In addition, a molecular mechanics Poisson-Boltzmann Surface Area (MM-PBSA) analysis was performed and the perturbation of the free energy and the decomposition of the energy contribution per residue were calculated to confirm the inhibitory effect of the compound Ignaciomyacin.

2. Material and methods

2.1. Ligand preparation

The newly derived geldanamycin analogue compound named Ignaciomyacin, which was isolated from terrestrial *Streptomyces* sp. CFR16 was chosen for computational studies to predict its efficacy against COVID-19. The structural configuration of the Ignaciomyacin (CCDC Deposition Number: 2218814) was obtained from single-crystal X-ray diffraction (XRD) analysis (Pachaiyappan, 2022) (Fig. 1). The conformer PDB format structure was derived, and its frontier HOMO, LUMO orbitals energies, and electrostatic potential was computed using the Gaussian09 program with density functional theory (DFT) and the basis set of B3LYP/6-31G(d,p) (M. J. Frisch, 2016, R.D. Dennington, 2016). Besides, Hirshfeld surface analysis was calculated to analyze the inter- and intramolecular interactions using CrystalExplorer-3.1 (Spackman et al., 2021).

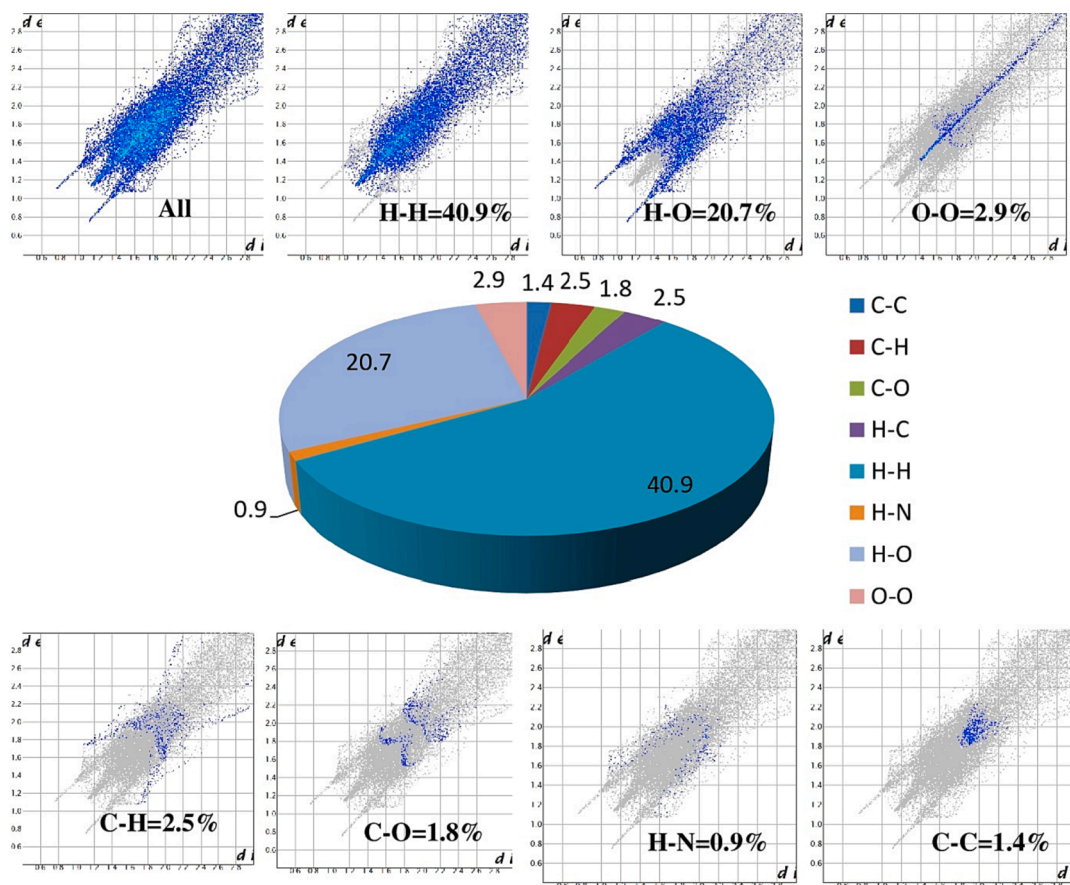


Fig. 3. Intramolecular atomic structural interaction analysis. Two-dimensional (2D) Fingerprint plot overall interactions and individual interactions in crystal packing of Ignaciomyacin.

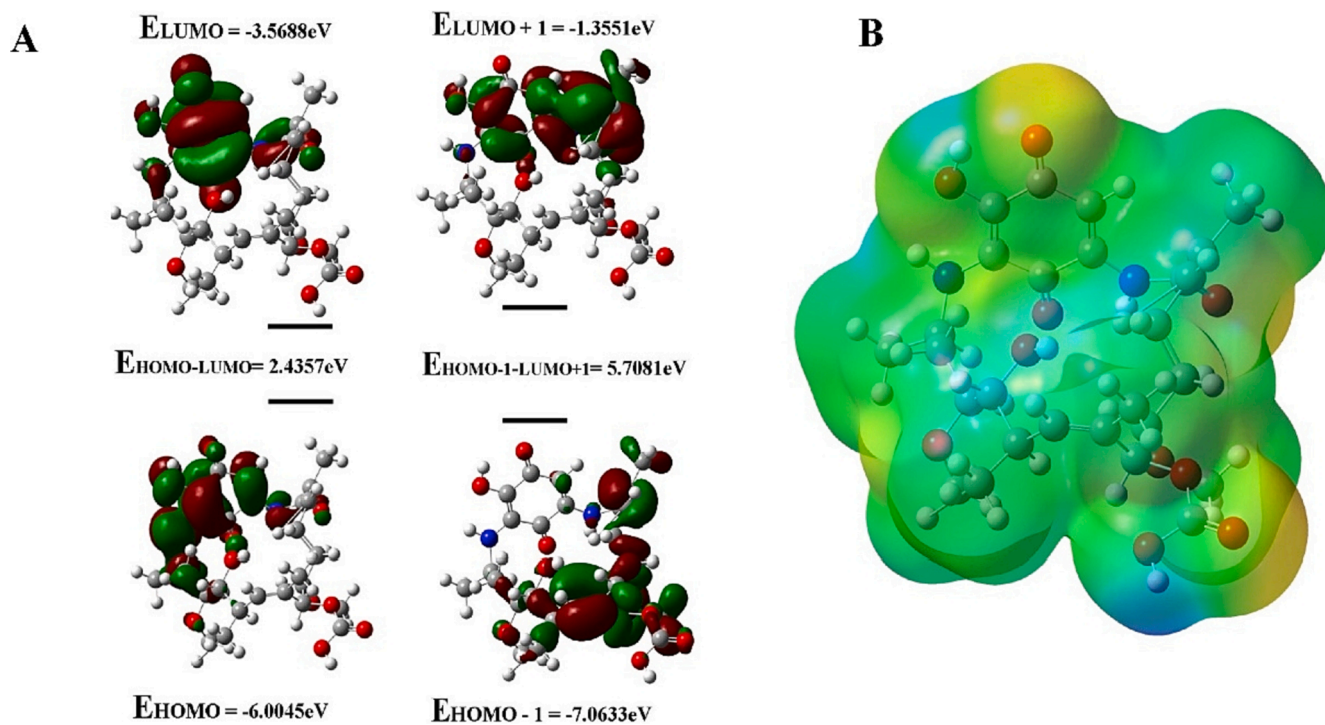


Fig. 4. HOMO and LUMO energy calculation. (A) Electron density distribution and the energies (eV) of HOMOs and LUMOs of Ignaciomyacin (The red and green colors represent the positive and negative phases of the molecule, respectively). (B) The 3D molecular electrostatic potential surface identifies the active sites for electrophilic and nucleophilic attack for Ignaciomyacin in optimized geometry.

Table 1
Calculated energy values of Ignaciomycin by B3LYP/6-31G (d,p) method.

Compound	Ignaciomycin
EHOMO (eV)	-6.0045
ELUMO (eV)	-3.5688
ELUMO-EHOMO	2.4357
Chemical Potential μ (eV)	-4.787
Chemical Hardness η (eV)	1.21785
Electrophilicity ω (eV)	9.407
Chemical Softness S (eV)	0.411

2.2. Protein preparation and molecular docking

The Receptor binding domain (RBD) of the SARS-CoV-2 spike glycoprotein of the wild-type (PDB ID:6M0J), Delta variant (PDB ID:7V8B), and Omicron variant (PDB ID: 7T9L) was chosen for this study. The structures were loaded into AutoDock software (Morris et al., 2009), water molecules and co-crystallized compounds were removed, and polar and nonpolar hydrogens, Kollman charges, and Gasteiger charges were added. COACH and CASTP servers (Dundas et al., 2006, Yang et al., 2013a, Yang et al., 2013b) were used to define the active sites. Then, the ligand parameters were included, and grid boxes (the number of grid points 100x100x100) were formed to cover the active sites. Further, the coordinates of the XYZ grid dimensions were set for the wild-type (x-33.507, y-30.09, z-8.015), Delta variant (x-186.556, y-193.596, z-278.008), and Omicron variants (x-228.181, y-175.319, z-251.794) with the default distance (0.375 Å) parameters.

The prepared ligand and proteins were used for the molecular docking analysis using autoDock4 (Morris et al., 2008, Stalin et al., 2020, Stalin et al., 2022b). The protein molecule's rigidity was maintained, and the ligand molecule was treated flexibly. The default docking parameters and Lamarck's Genetic Algorithm were used to run the docking for 250,000 evaluations. The least energy-docked confirmations of ligand-protein complexes were screened, and their interactions were analyzed.

2.3. Molecular dynamics simulation

After the docking analysis, the finalized complex of the compound Ignaciomycin with the RBD of the SARS-CoV-2 spike glycoprotein of the wild-type, Delta variant, and Omicron variant was used for the

molecular dynamics simulation (GROMACS-2018.6 package) (Van Der Spoel et al., 2005, Abraham et al., 2015, Stalin et al., 2022a) to determine the conformational trajectory changes in the proteins.

The ligand topology was generated using the CHARMM General Force Field (CGenFF) server 4.6 (Vanommeslaeghe et al., 2010) and the protein topology was developed with the CHARMM36-jul2021 force-field (Huang et al., 2017). The system was neutralized with 0.15 M sodium chloride ions. Then, the system was energy minimized with 50000 ns steps using the steepest descent minimization algorithm. Then, the system was equilibrated by the NVT (substance amount, volume, and temperature) and the NPT (substance amount, pressure, and temperature) ensembles at 300 K and 1.0 bar pressure for 50000 ns steps each with the Particle Mesh Ewald (PME) coulomb type and Verlet cut-off scheme (Darden et al., 1993). Then, the system performed a ~ 100 ns simulation in the ubuntu server 20.04 LTS with an Intel(R) Xeon(R) CPU E5-2620 v3 @ 2.40 GHz processor. Grace Plotting Tool (<https://plasma-gate.weizmann.ac.il/Grace/>) was used to analyze the simulation data and develop the figures for RMSD (root mean square deviation), RMSF (root mean square fluctuation), the average number of H-bonds, the solvent-accessible surface area, and the radius of gyration. Data analysis of the covariance matrix and free energy landscape (FEL) was developed using the gmX anaig and sham tools, and the associated eigenvectors and positions of the lowest energy conformations were determined. Discovery Studio 2021 client, PyMol, and UCSF Chimera 1.16 tool were used to visualize the binding information of the docked and simulated structures and Mathematica software was used to generate the FEL plots.

2.4. Molecular mechanics Poisson-Boltzmann surface area (MMPBSA) analysis

To determine the free energy binding affinity, the last 2000 frames of the 100 ns simulated complex of the compound Ignaciomycin and the three RBD of the SARS-CoV-2 spike glycoprotein of the wild-type, Delta variant, and Omicron variant were analyzed by g_MMPBSA software (Kumari et al., 2014) using Molecular mechanics Poisson – Boltzmann surface area (MM-PBSA) calculations.

Table 2
Protein-Protein interaction analyses of the SARS-CoV-2 S-glycoprotein and ACE2-receptor of the wild-type, delta and omicron-variants.

Potential Hydrogen Bonds				SARS-Cov-2-S RBD–Wild-type*				Type of H-Bond	Distance (D-A)\AA
ACE2 ResNum	ResName	Chain-1	AtomName	ResNum	ResName	Chain-2	AtomName		
24	GLN	A	OE1	487	ASN	E	ND2	SS	2.69
30	ASP	A	OD2	417	LYS	E	NZ	SS	2.90
42	GLN	A	NE2	446	GLY	E	O	SB	3.24
42	GLN	A	NE2	449	TYR	E	OH	SS	2.79
353	LYS	A	O	502	GLY	E	N	BB	2.78
353	LYS	A	NZ	496	GLY	E	O	SB	3.08
ACE2				SARS-Cov-2-S RBD – Delta				Type of H-Bond	Distance (D-A)\AA
ResNum	ResName	Chain-1	AtomName	ResNum	ResName	Chain-2	AtomName		
38	ASP	F	OD2	449	TYR	A	OH	SS	3.19
31	LYS	F	NZ	493	GLN	A	OE1	SS	3.26
353	LYS	F	NZ	496	GLY	A	O	BS	2.63
41	TYR	F	OH	500	THR	A	O	BS	2.66
ACE2				SARS-Cov-2-S RBD – Omicron				Type of H-Bond	Distance (D-A)\AA
ResNum	ResName	Chain-1	AtomName	ResNum	ResName	Chain-2	AtomName		
38	ASP	D	OD2	449	TYR	A	OH	SS	3.23
35	GLU	D	OE2	493	ARG	A	NH1	SS	2.69
38	ASP	D	OD1	498	ARG	A	NH1	SS	3.17
353	LYS	D	O	502	GLY	A	N	BB	2.99

* The interactions between the S-glycoprotein of the wild-type with the ACE2-receptor were already analyzed, and the data are displayed here for reference [15].

Table 3
Various interactions of Ignaciomyacin with the RBD of the SARS-CoV-2 S-glycoprotein in wild-type, delta and omicron-variants.

Ligand	Protein	Interacting residues & atoms in bond (ligand - Receptor)	Interaction type	Distance	Binding Energy (kcal/mol)	Vdw_hb_desolv_energy (kcal/mol)	Inhibition constant	Ligand efficiency
Ignaciomyacin	6MOJ - wild-type	TYR453 (OH-OAN)GLY496 (N-OAH)TYR505 (OH-OBB)GLN493 (OEL:B-HAL)SER494 (O-HAL)TYR449 (OH-HAI)	H-Bond: Conventional H-BondH-Bond: Conventional H-BondH-Bond: Conventional H-BondH-Bond: Conventional H-BondH-Bond: Conventional H-Bond	3.01292,73012.61952.09012.61772.3543	-6.58	-7.20	80.88 (uM)	0.23
		GLN493 (HE2I-OBG)ASN501 (ODI-HAI)PHE497 (HA-OAG)SER494 (OG-CBH)TYR449 (OH-CAS)GLY496 (O-CAS)TYR505	H-Bond: Conventional H-BondH-Bond: Carbon H-BondH-Bond: Carbon H-BondH-Bond: Carbon H-BondHydrophobic: Pi-Pi T-shaped	2.59531.85952.16063.07363.10013.67174.8145	-7.02	-6.07	208.33 (uM)	0.26
		SER496 (OG-OBB)ARG498 (NH1-OBB)ARG498 (NH1-OBG)ARG498 (NH2-OBD)TYR501 (OH-OBG)HIS505 (ND1-OAN)SER494 (O-HBS)TYR453 (OH)	H-Bond: Conventional H-BondH-Bond: Conventional H-BondH-Bond: Conventional H-BondH-Bond: Conventional H-BondH-Bond: Conventional H-BondH-Bond: Pi-Donor H-Bond	3.00663.17783.23412.48872.97472.63692.05173.4505	-8.65	-5.9	72.18 (uM)	0.29
Ignaciomyacin	7i9l-Omicron							

3. Results

3.1. Hirshfeld surface analysis

The structural configuration of the Ignaciomyacin (CCDC Deposition Number: 2218814) was obtained from single-crystal X-ray diffraction (XRD) analysis (Pachaiyappan, 2022) (Fig. 1). The surface and close contacts of atoms in Ignaciomyacin were studied by Hirshfeld surface analysis. The points on the molecular surface ranged from red to white to blue, showing intermolecular contacts with the corresponding inter-nuclear distance smaller, equal, and larger than the Van Der Waal radii. The d_{norm} , shape index, and curvedness of Hirshfeld molecular surface analysis for the compound Ignaciomyacin are shown in Figure (Fig. 2). These parameters are shown in ranges from -0.592 to 6.208 , -1.0000 to 1.0000 , and -4.0000 to 0.4000 , respectively.

Two-dimensional (2D) fingerprint diagrams were also constructed to analyze the intermolecular atomic contacts in the Ignaciomyacin crystal structure. The distance between the Hirshfeld surface and the nearest atomic nucleus within the surface is called the internal distance (d_i). The distance between the Hirshfeld surface and the outside of the surface is called the external distance (d_e). These two terms, d_i and d_e , in the 2D fingerprint diagram reveal more information about the molecular surface based on the interatomic contacts.

The 2D fingerprint diagrams show that intermolecular interactions such as H...H, H...O, O...O, C...H, N...H, and C...C clearly dominate the graphical Hirshfeld surfaces (Fig. 3). In addition to a 2D fingerprint map of Ignaciomyacin, Fig. 3 illustrates the percentage contribution of selected interatomic contacts to the Hirshfeld surface region for Ignaciomyacin. Using the most accurate 2D fingerprint diagrams available, the contribution of the intermolecular interactions H...H (40.9 %), H...O (20.7 %), O...O (2.9 %), C...H (2.5 %), C...O (1.8 %), H...N (0.9 %), and C...C (1.4 %) that make up the entire Hirshfeld surface is carefully examined. The entire Hirshfeld surface of the molecule was covered by the intermolecular interactions of H...H and H...O in proportions of 40.9 % and 20.7 %, respectively. The deep red spots on the d_{norm} Hirshfeld surfaces indicate that the main intermolecular hydrogen bonding is primarily due to H...O/O...H close-contact interactions.

The molecule contains an intramolecular hydrogen bond between O10 and H27a (2.552 Å). H...O/O...H contacts contribution is 20.7 %, which plays a substantial role in crystal packing. The set of 60 potential intermolecular hydrogen bonds, including long range of force of attractions, are responsible for packing the crystal, and the interactions are shown in the Supplementary section (SI Fig. 1).

3.2. HOMO-LUMO analysis

The energies of the frontier orbitals can be easily correlated with various parameters of the molecules. The larger the EHOMO value, the greater the molecule's ability to donate electrons, and the smaller the ELUMO value, the greater the ability to accept electrons. The considerable ΔE value indicates moderate kinetic stability and lowers chemical reactivity. The electronic transition absorption corresponds to the transition from HOMO to LUMO by electron transfer (Fig. 4A).

In the compound Ignaciomyacin, the electron density of HOMO (-6.0045 eV) is distributed over the quinone and the adjacent side chain. At the same time, HOMO -1 (-7.0633 eV) of Ignaciomyacin is mainly distributed over the carbonyl group involved in conjugation with the double bonds of the side chain. The LUMO (-3.5688 eV) is primarily located on the quinone ring and is weakly distributed over a close side chain with an amide bond. The LUMO $+1$ (-1.3551 eV) is distributed over the quinone ring and is partially distributed over the close side chain. The calculated HOMO-LUMO energy gap is 2.4357 eV (Fig. 4A).

3.3. Chemical reactivity

The frontier orbital energies clearly show various properties, such as

Table 4
The binding free energy values of Ignaciomyacin with wild-type, delta, and omicron-variants.

Complex	Binding free energy(kJ/mol)	Electrostatic energy (kJ/mol)	Van der Waal energy(kJ/mol)	Polar solvation energy(kJ/mol)	SASA energy(kJ/mol)
Wild-type-Ignaciomyacin	-75.599+/-0.541	-284.686+/- 0.402	-1.662+/-0.282	215.114+/-0.623	-4.358+/-0.025
Delta-Ignaciomyacin	-178.494+/-0.858	-395.904+/- 0.673	-9.806+/-0.391	232.623+/-1.022	-5.375+/-0.034
Omicron-Ignaciomyacin	-237.658+/-0.375	-560.012+/- 0.490	-24.975+/-0.414	356.902+/-0.500	-9.575+/-0.028

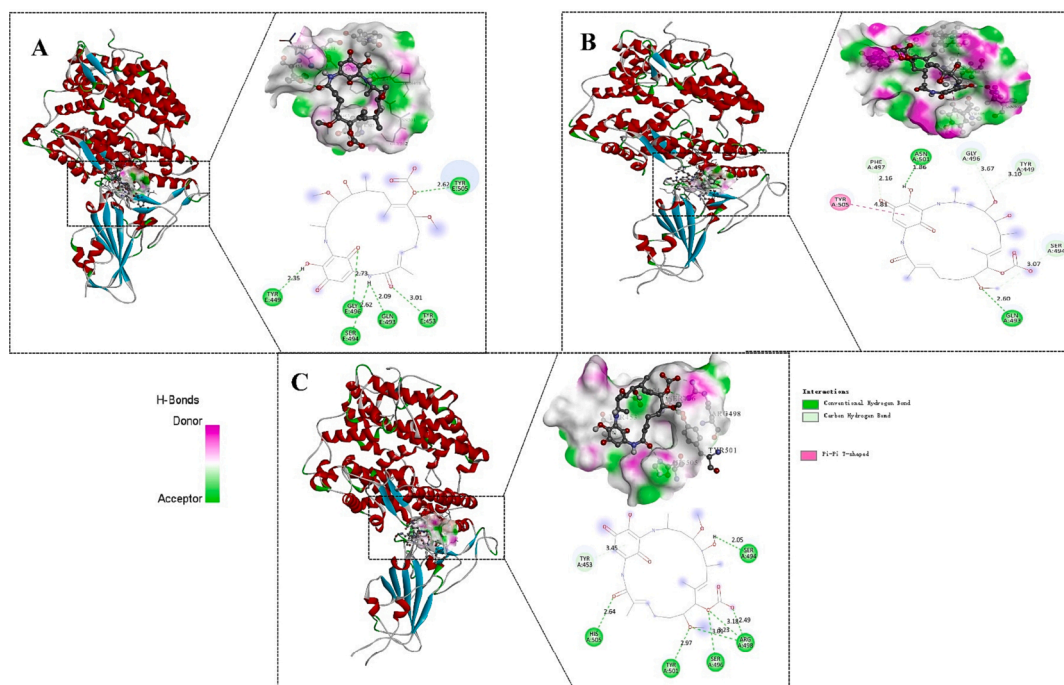


Fig. 5. Molecular docking (Ligand-protein) interaction. The interaction with the least energy mode of Ignaciomyacin with the RBD of SARS-CoV-2 S-glycoprotein placed in the cavity of the surface region of the (A) wild-type, (B) delta-variant, (C) omicron-variant.

chemical potential (μ), chemical hardness (η), and electrophilicity index (ω), which are listed in Table 1. The above properties are calculated using HOMO and LUMO energies with the help of the Koopmans theorem and Parr approximation.

$$\mu = (EHOMO + ELUMO)/2 \quad (1)$$

$$\eta = (ELUMO - EHOMO)/2 \quad (2)$$

$$\omega = \mu^2 / 2\eta \quad (3)$$

$$\text{Chemical softness } S = 1/(ELUMO - EHOMO) \quad (4)$$

The electrophilicity index (ω) indicates the stabilization energy of the molecule, which readily accepts the electronic charge from the adjacent environment and it is preferred to undergo the electrophilic reaction with the circumstances. The aromatic ring substituents with a long chain in Ignaciomyacin led to a greater effect of electrophilic reaction in their singlet ground state ($\omega = 9.407$ eV). The considerable hardness (η) of Ignaciomyacin is 1.2179 eV, indicating moderate reactivity of Ignaciomyacin with less accessible polarizability and a very low chemical softness (Table 1). A rigid molecule with a substantial HOMO-LUMO gap with high excitation energies was essential for various excited states; it was less reactive, and the electron density was more difficult to change than for a soft molecule.

3.4. Electrostatic potential analysis

The molecular surface with red markings has a high negative ESP surface (electron-rich centers) and acts as a nucleophilic center. The molecular surface with blue hues has a positive ESP surface (electron-poor centers) and serves as an electrophilic center. Green shades represent neutral sites. Thus, the molecular electrostatic potential calculation was assessed to identify the active sites for electrophilic and nucleophilic attack for Ignaciomyacin in optimized geometry. As shown in Fig. 4B, the blue < green < red sequence on the molecular surface of Ignaciomyacin shows an increasing potential, indicating various sites of negative nature at O1 and O3 in the quinone ring, O4 of the amide and O6, O7, O8 of the carboxylic acid. Positive nature is easily found at H2 of the amine, H2a of the hydroxyl group, and H7 of the carboxylic acid atoms of butyrolactone ring. These positive centers in systems can interact with nucleophilic centers and are involved in H-bonding with proteins of pathogens.

3.5. Protein-Protein interaction

Here, we investigated the H-bonding interactions between the S-glycoprotein of Delta and Omicron with the ACE2-receptor (Table 2). In the Delta, Tyr449, Gln493, Gly496, and Thr500 showed H-bonds with Asp38, Lys31, Lys353, and Tyr41; in Omicron, Tyr449, Arg493, Arg498, and Gly502 showed H-bonds with Asp38, Glu35, Asp38, and Lys353, with the ACE2-receptor. Interestingly, no hydrophobic interactions, salt-bridges, and unfavorable electrostatic interactions with the ACE2-

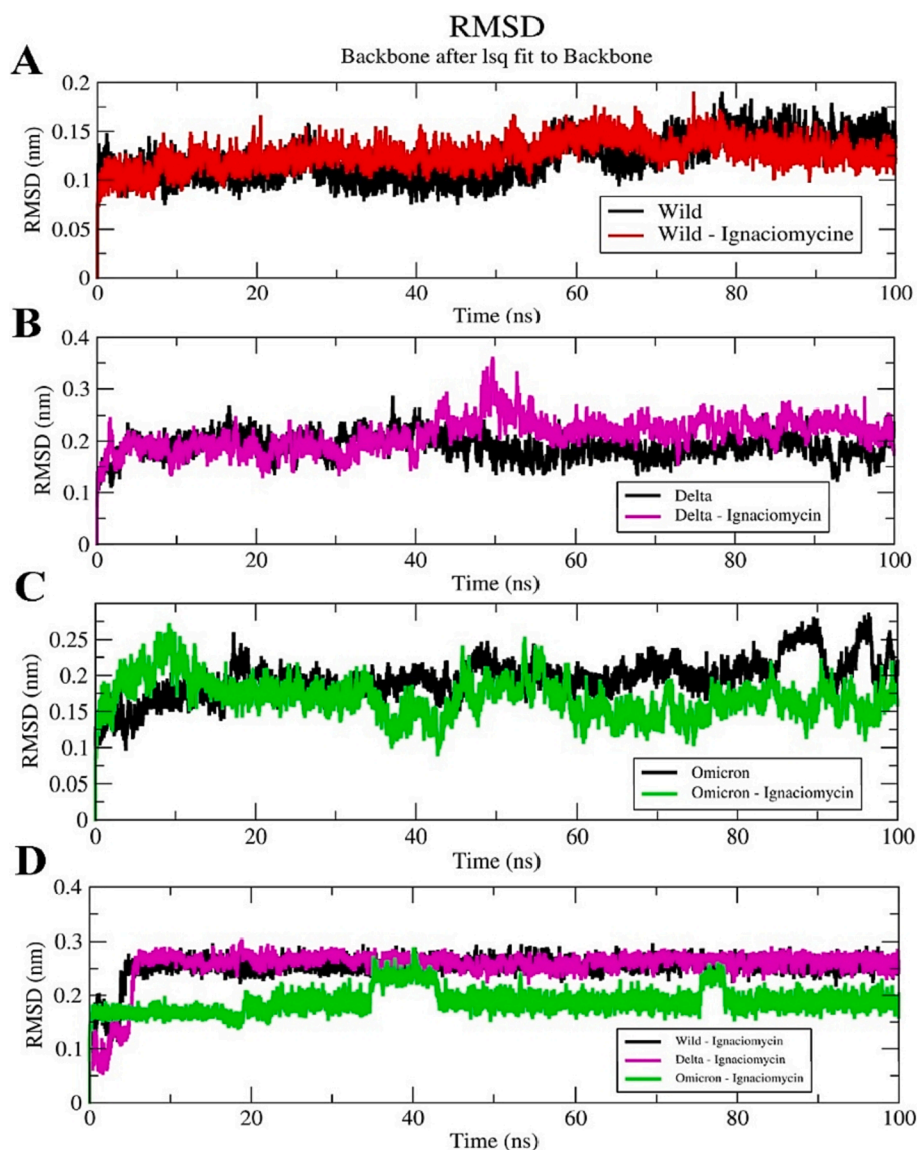


Fig. 6. Root Mean Square Deviation (RMSD) plot. (A) Ignaciomyicin-wild-type. (B) Ignaciomyicin-delta. (C) Ignaciomyicin-omicron. (D) Ignaciomyicin alone in all the three complexes.

receptor occurred with Delta (SI-Table 2). The Omicron-ACE2-receptor complex formed the hydrophobic interaction Phe486-Leu79, similar to wild-type, but there was no H-bonding between Asn487-Gln24. This was because of the other mutation that occurred in the RBD of the Omicron and the potential short contacts formed between Gly476-Gln24 and Tyr501-Tyr41 (SI Table 3). The Phe486-Leu79 hydrophobic interaction contributes to the segregation of the nonpolar residues and induces H-bonding between Asn487-Gln24 in the wild-type but not in the Delta.

3.6. Docking analysis

The ADMET properties of Ignaciomyicin were analyzed using OSIRIS-DataWarrior (SI-Table 4) (Lopez-Lopez et al., 2019). The modification of Geldanamycin at the quinone ring can increase its potency, metabolic stability, and water solubility. The hydroxyl (OH) group was added to the benzoquinone moiety and carboxylic acid groups in the 10th position of Ignaciomyicin, which may result in lower metabolic toxicity and higher potency and water solubility compared to Geldanamycins (SI Table 4) and could lead to an improvement in metabolic potency. Ignaciomyicin has 5H-bonding donors and 12H-bonding acceptors and has good drug-likeness (7.5912) compared to Geldanamycin. Both

cLogP (1.4933) and cLogS (-3.502) indicate that the hydrophilicity and water solubility of Ignaciomyicin were improved. Moreover, it shows no adverse effects such as mutagenic, tumorigenic, reproductive, or irritant effects. However, experimental studies are needed to confirm its stability and toxicity.

Upon docking at the RBD-ACE2 interface, Ignaciomyicin formed a strong conventional and carbon H-bonding with amino acid residues Tyr453, Gly496, Tyr505, Gln493, Ser494, and Tyr449 in the wild-type (Fig. 5A), Gln493, Asn501, Phe497, Ser494, Tyr449, and Gly496 in the Delta (Fig. 5B) and Ser496, Arg498, Tyr501, His505, and Ser494 in the Omicron (Fig. 5C), respectively. The least energy-confirmed poses of docked complexes were selected for further analysis and all interactions are listed in Table 3.

3.7. MD simulation

RMSD plotting of Ignaciomyicin-RBD in the wild-type and Delta showed that residues converged and structural stability was maintained throughout the simulation period (Fig. 6A, B). For Delta, there was a structural deviation and upward shift of ~ 50 ns, which then typically converged the rest of the simulation (Fig. 6B). For Ignaciomyicin-

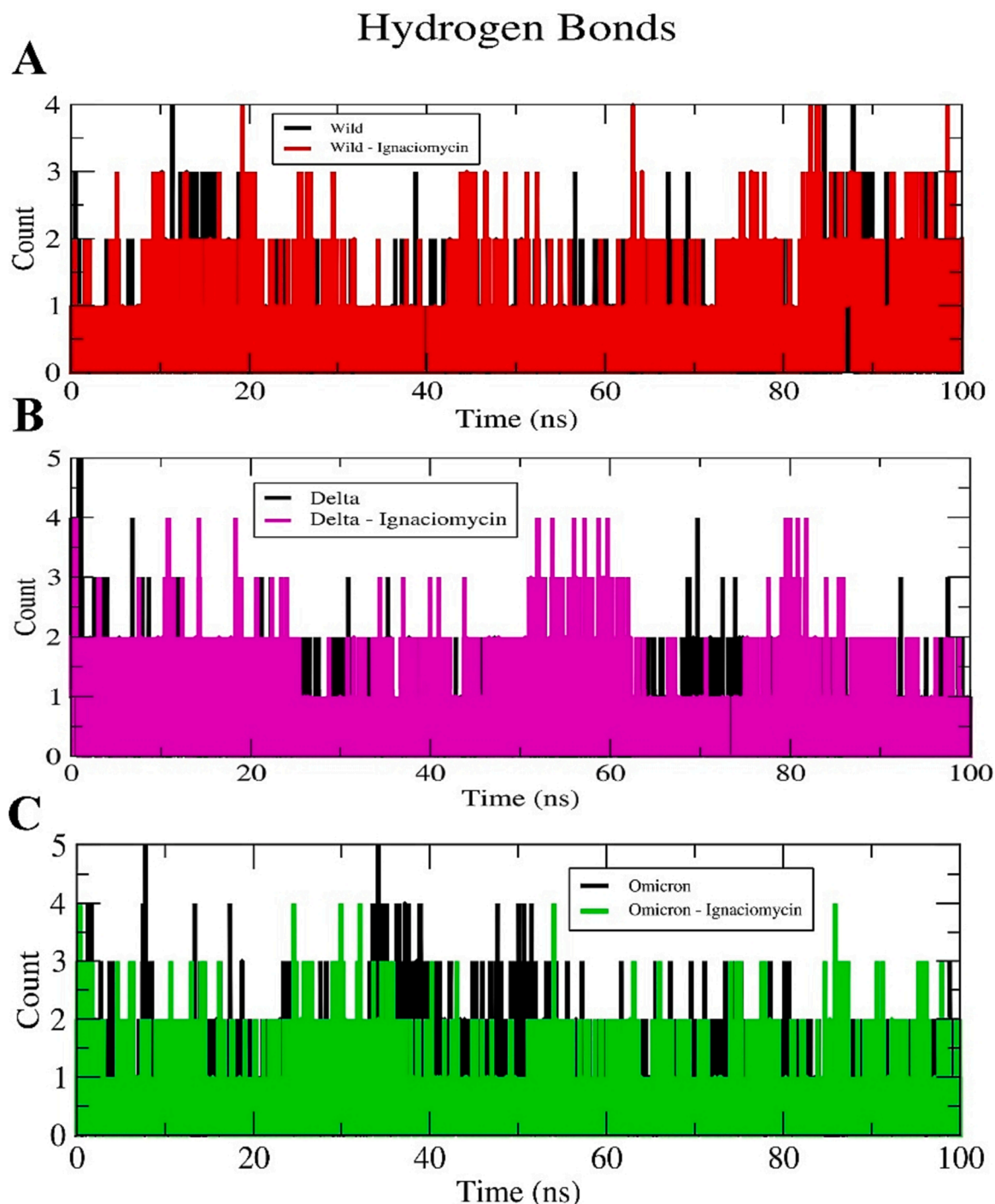


Fig. 7. Intermolecular Hydrogen bond plot. (A) Ignaciomyacin-wild-type. (B) Ignaciomyacin-delta. (C) Ignaciomyacin-omicron.

Omicron, there was a structural deviation upward at ~ 20 ns and then a significant structural deviation was observed throughout the simulation. These deviations were due to the mutations and the strong interaction of the Ignaciomyacin in the RBD region (Fig. 6C). The backbone RMSD of Ignaciomyacin confirmed its stability (Fig. 6D) and the Apo wild-type, Delta, and Omicron confirmed the structural variation due to the mutations (SI Fig. 2).

In all three complexes, Ignaciomyacin maintained its stability throughout the simulation and retained strong conventional H-bonding and other interactions, similar to docking analysis (SI Figs. 3, 4, 5); these interactions significantly altered the RBD region of wild-type, Delta, and Omicron, and confirmed by secondary structure analysis (SI Figs. 6, 7,

8). The number of intermolecular H-bond contacts of all three complexes is shown in Fig. 7.

The dynamic behavior of the individual residues was investigated based on the RMSF of all complexes. The combined H-bonds and hydrophobic interactions were reflected as residual fluctuations in the RMSF plots of all simulated complexes, especially in the corresponding active and mutant residues of the RBD region (Fig. 8). Compared to the wild-type, the residues at both the N- and C-terminus of the Delta and Omicron variants showed flexibility during the simulation period. In particular, the flexibility is greater in the RBD region due to the mutation and it was even greater during the interaction of Ignaciomyacin in the apo and complex structures. These fluctuations can be seen in the RMSF of

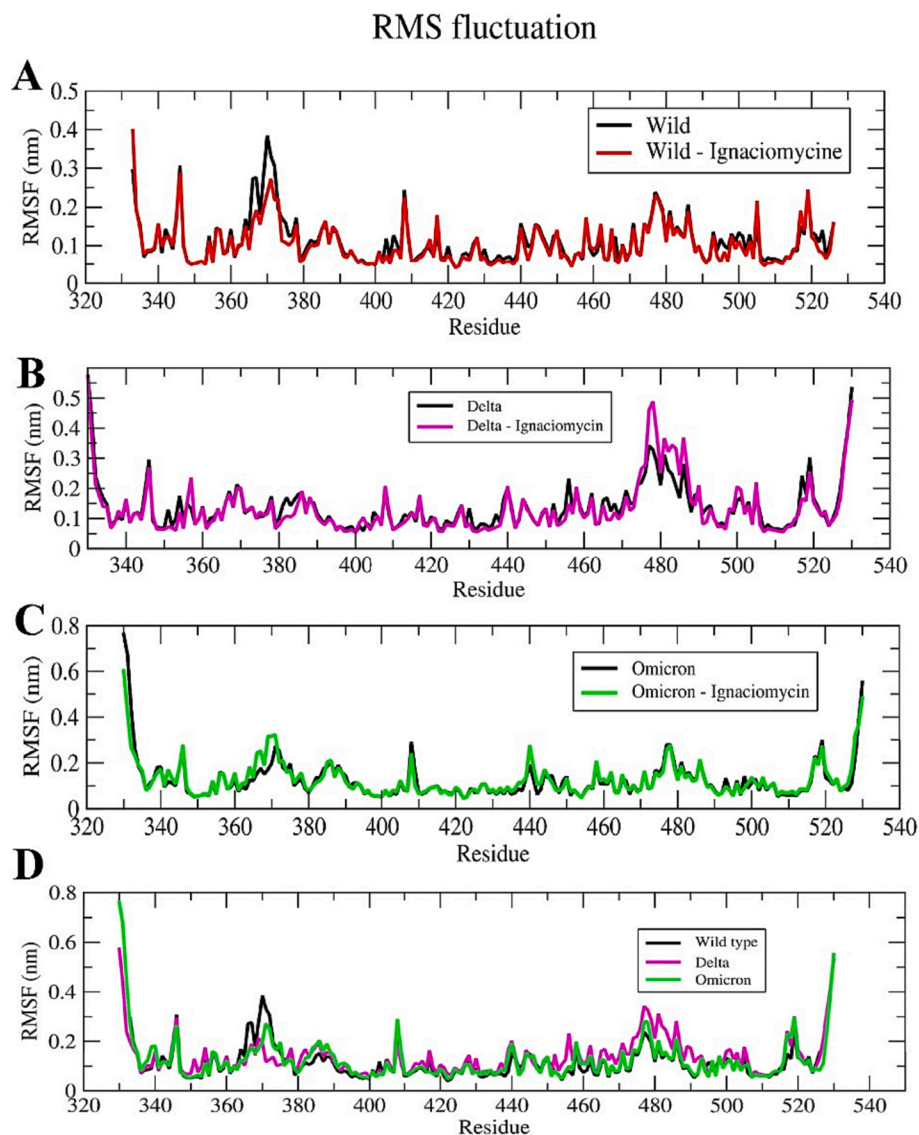


Fig. 8. Root Mean Square Fluctuation (RMSF) plot. (A) Ignaciomyacin-wild-type. (B) Ignaciomyacin-delta. (C) Ignaciomyacin-omicron. (D) superimposed RMSF plot for wild-type. (E) delta and omicron-variants alone.

the mutant residues of the Delta (Arg452 and Lys478) (Fig. 8B, D) and Omicron (Leu371, Phe373, Lys440, Arg493, Ser496, Arg498, Tyr501 and His505) (Fig. 8C, D) variants.

3.8. Covariance and PCA analysis

The diagonal matrix of five eigenvectors and their eigenvalues for each complex and the apo state were summarized based on the RMSD and RMSF projections (SI Figs. 9, 10, 11), and the atomic fluctuations in the collective motions of each particle in the S-glycoprotein and RBD regions were analyzed. Each of the collected eigenvectors defined the corresponding atom contributing to the collective motion of particles per atom (Figs. 9, 10, 11).

In the wild-type, based on the collective motion particles, there was atomic motion in the core region of the N-terminal and the β 1- and β 2-sheets. Similarly, a slight particle fluctuation was observed in the β 6 sheets of the RBM region (Fig. 9A, B). After interaction with Ignaciomyacin, particle motion was slightly altered in the core region of N-terminus. Atomic fluctuations were observed in the β 6-, β 3- and β 5- sheets and opposite manner in the β 1-, and β 2-sheets (Fig. 9C, D).

The Delta-variant showed large collective motion particles in β 5- and

β 6-sheets in the RBM region. These fluctuations probably occurred due to mutation in residues Leu452Arg and Thr478Lys. Moreover, there were fluctuations and opposing movements in the core region of N-terminus and residues in most β -sheets (Fig. 10A, B). A contradictory large atomic rotational drift was observed at the RBM, the core region of N-terminus, and most β -sheets after Ignaciomyacin interaction (Fig. 10C, D).

In the Omicron-variant, slight particle motions were observed in the RBM region, due to the mutated non-polar and positively charged amino acids and their enhanced hydrophobic surface in the RBM regions. Simultaneously, opposite atomic motions and fluctuations were observed in the core region of the N-terminus and a slight drift across residues in most β -sheets similar to the Delta-variant (Fig. 11A, B). After interaction with Ignaciomyacin, there were many atomic rotational drifts and significant fluctuations in the collective motion particles in an anticorrelated manner in the RBM region and the core region of N-terminal, respectively. Moreover, most of the existing atoms in β -sheets were moved in a partially correlated and anti-correlated manner. This large number of collective motions is due to the strong interaction of Ignaciomyacin with the non-polar and positively charged mutant amino acids in the RBM region of the Omicron-variant (Fig. 11C, D).

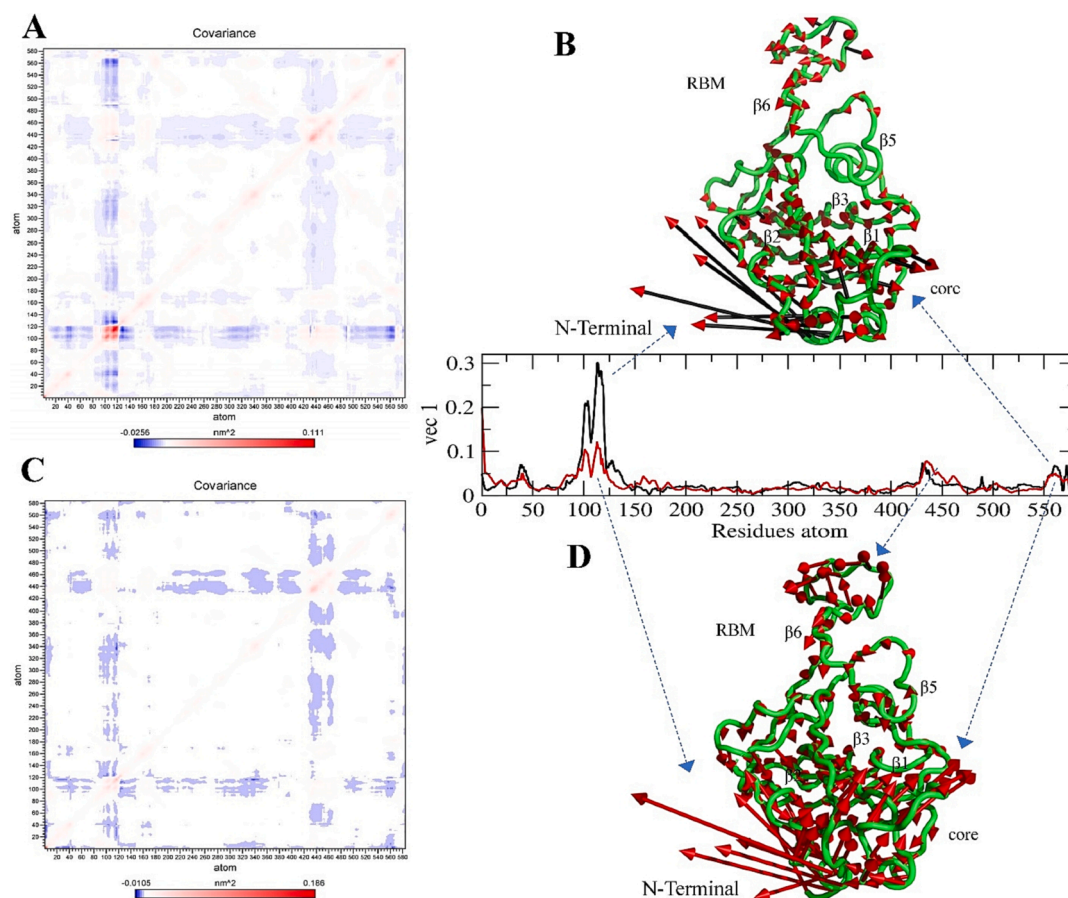


Fig. 9. Covariance and Principal Component Analysis of Wild-type. (A, B) Total atom fluctuation and motility analyzed by covariance matrix and PCA for the apo wild-type and (C, D) Ignaciomyacin-wild-type; (B) the black and red arrow marks indicate the atomic motion in the wild-type; (D) the full red color indicates the atomic motion in the Ignaciomyacin-wild-type; in the covariance matrix, (A, C) the red color indicates the interacting two atoms are moving together, and blue indicates atoms moving on the opposite side.

In addition, free energy landscape analysis was used to analyze the confirmations of the lowest energy of wild-type, delta and omicron along with the binding of Ignaciomyacin based on the PC1 and PC2 plots with the comparison of RMSD and Radius of Gyration against Gibbs free energy. The overall FEL plots of all variants are shown in the figure (Fig. 12). There are large and small confirmations of the lowest energy obtained in the wild type, whereas, in the wild-type Ignaciomyacin complex, there is a large energy distribution obtained in the minimal cluster (Fig. 12A). In contrast, two differentials' confirmations of lowest energy were obtained in both the delta and delta-Ignaciomyacin complexes, but the delta-Ignaciomyacin complex showed the lowest energy intense to the minimal cluster (Fig. 12B). The omicron and omicron-Ignaciomyacin complexes showed a single minimal energy cluster, but the omicron-Ignaciomyacin complex showed a strong large distribution in the minimal cluster (Fig. 12C). These particular free energy confirmations distributed different energy clusters due to the mutations and interaction of Ignaciomyacin reduced the residual fluctuation and developed the minimal energy distribution in the principal components of all complexes. These results are also confirmed by the analysis of the eigenvectors associated with the covariance matrix.

Furthermore, changes in the solvent-accessible surface area (SASA) and the average area per residue in the overall simulation were calculated and confirmed the stability of Ignaciomyacin (SI Fig. 12, 13, 14).

3.9. Free energy binding analysis

The last 2000 frames of ~ 100 ns simulated complexes were used to determine the contribution of binding free energy and decomposition of

each residue in the interaction of Ignaciomyacin with all the three variants (Table 4). The ΔG -binding energy of the complexes Ignaciomyacin with the wild-type, delta, and omicron variants was determined to be -75.602 ± 24.417 kJ/mol, -178.487 ± 37.302 kJ/mol and -237.671 ± 16.456 kJ/mol, respectively.

The free ΔG -binding energy of Ignaciomyacin with Delta and Omicron showed comparatively and significantly the highest binding value, confirming the strong interaction of Ignaciomyacin and blocking of RBD-ACE2 interaction due to the mutation (Fig. 13B, C). Simultaneously, Ignaciomyacin also showed a better ΔG -binding free energy for the wild-type (Fig. 13A). Moreover, Ignaciomyacin showed significant electrostatic and polar solvation energy with all variants.

4. Discussion

The severity of viral infections is usually determined by where mutations occur in the virus's genetic material and affect its functional properties. Because the natural variant of SARS-CoV-2 has infected a larger number of people, the mutant variants have now also caused significant problems. The new mutant variants of SARS-CoV-2 are highly contagious compared to the native virus, and the Omicron variant, in particular, is one of the most important (Lupala et al., 2022). The N-terminal S-glycoprotein, especially the RBD of SARS-CoV-2, has strong H-bonds and electrostatic interactions with the binding domain of the human ACE2-receptor (Tortorici and Veessler, 2019).

In this current study, we investigated the interactions between the SARS-CoV-2 S-glycoprotein of Delta and Omicron with the ACE2-receptor and the findings were compared with the previously

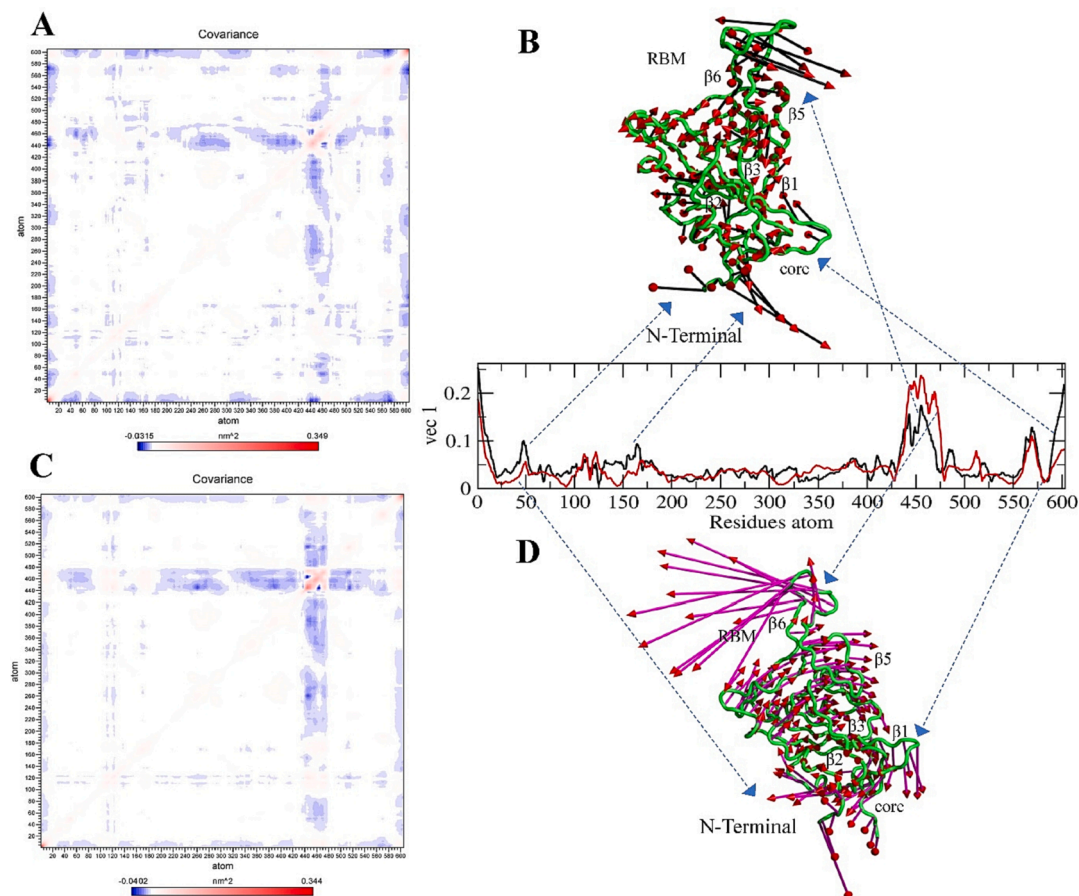


Fig. 10. Covariance and Principal Component Analysis of Delta variant. (A, B) Total atom fluctuation and motility analyzed by covariance matrix and PCA for the apo delta and (C, D) Ignaciomylin-delta; (B) the black and red arrow marks indicate the atomic motion in the delta; (D) the full magenta with red color indicates the atomic motion in the Ignaciomylin-delta; in the covariance matrix, (A, C) the red color indicates the interacting two atoms are moving together, and blue indicates atoms moving on the opposite side.

published wild-type data (Lan et al., 2020, Stalin et al., 2022b). The Omicron showed significant conformational changes in the RBD compared to the wild-type, based on the critical mutations at residues in the RBD, such as Asn417, Asp339, Lys440, Leu371, Phe373, Phe375, Ser446, Asn477, Lys478, Ala484, Arg493, Ser496, Arg498, Tyr501, and His505, which significantly altered the electrostatic surface of the RBD-ACE2 interface due to the large side chains of mutant amino acids such as Lys440 and Lys478 (Yang et al., 2021). These mutants Arg493, Lys478, and Arg498, generated positive charges in the RBD interface of the Omicron and strongly interacted with ACE2, which had negatively charged amino acids such as Glu35 and Asp38. Besides, the RBD of the Delta exhibited mutations in Arg452 and Lys478, which are also generated positive charges (Li et al., 2021, Lupala et al., 2022).

Moreover, Omicron formed the salt-bridge between Arg493-Glu35 and Arg498-Asp38 and also formed the unfavorable electrostatic interactions between Arg403-Lys353, Arg493-Lys31, Arg493-His34, Arg498/His505-Lys353. Besides, some favorable electrostatic interactions and short contacts in Delta and Omicron were also analyzed, which differed from the wild-type (SI Table 3). In our previous alanine scanning mutagenesis study (Stalin et al., 2022b), we predicted that important residues such as Lys417, Tyr449, Tyr453, Leu455, Phe456, Gln493, Gln498, Thr500, Asn501, and Tyr505 were responsible for stabilizing the S-glycoprotein-ACE2-receptor complex in wild-type. Some predicted residues were confirmed by Omicron, such as Lys417Asn, Gln493Lys, Gln498Arg, Asn501Tyr and Tyr505His. The mutants Asn417, Lys440, Arg493, and Arg498 altered the electrostatic surface in the RBD of Omicron and increased ACE2 interaction affinity and decreased vaccine affinity (Yang et al., 2021). However, the mutant

residues Arg452 and Lys478 in the Delta did not interact with the ACE2-receptor but caused conformational changes in the protein (Goher et al., 2021, Zhao et al., 2022).

The above-mentioned amino acids present in the RBD of wild-type, Delta and Omicron are the main active sites for inhibiting SARS-CoV-2 inhibition. Therefore, it is important to check the interaction of drugs or natural compounds with these active sites. Geldanamycin is a benzoquinone and belongs to the ansamycins group with known antimicrobial and anticancer activities. Since Geldanamycin exhibits hepatotoxicity due to the benzoquinone moiety, effective doses and uses are limited (Taechowisan et al., 2020, Skrzypczak et al., 2021). Geldanamycin and its derivatives are potent inhibitors of heat shock protein 90 (HSP90) and inhibit most viruses such as influenza virus, HIV-1, and herpes by altering the host response (Connor et al., 2007, Li et al., 2012, Sultan et al., 2020). For viral replication, HSP90 plays an important role in viral protein synthesis. Recent research has shown that geldanamycin blocks viral replication by inhibiting HSP90 (Connor et al., 2007, Li et al., 2012, Sultan et al., 2020, Kasperkiewicz, 2021). Some geldanamycin derivatives modified at positions C17 and C19 showed their antiviral activity against the influenza virus, HIV-1, hepatitis C and B, and herpes (Connor et al., 2007, Qu et al., 2011, Kousara et al., 2017, Taechowisan et al., 2020). Therefore, we speculate that Ignaciomylin, the analogue of geldanamycin, may also inhibit HSP90 and block viral replication and also act as an anticancer agent. However, we focused on determining the efficacy of Ignaciomylin in inhibiting SARS-CoV-2 and its mutations through molecular docking and dynamics simulation analyses and confirmed its inhibitory activity. Based on this docking analysis, Ignaciomylin was found to form interactions with the major

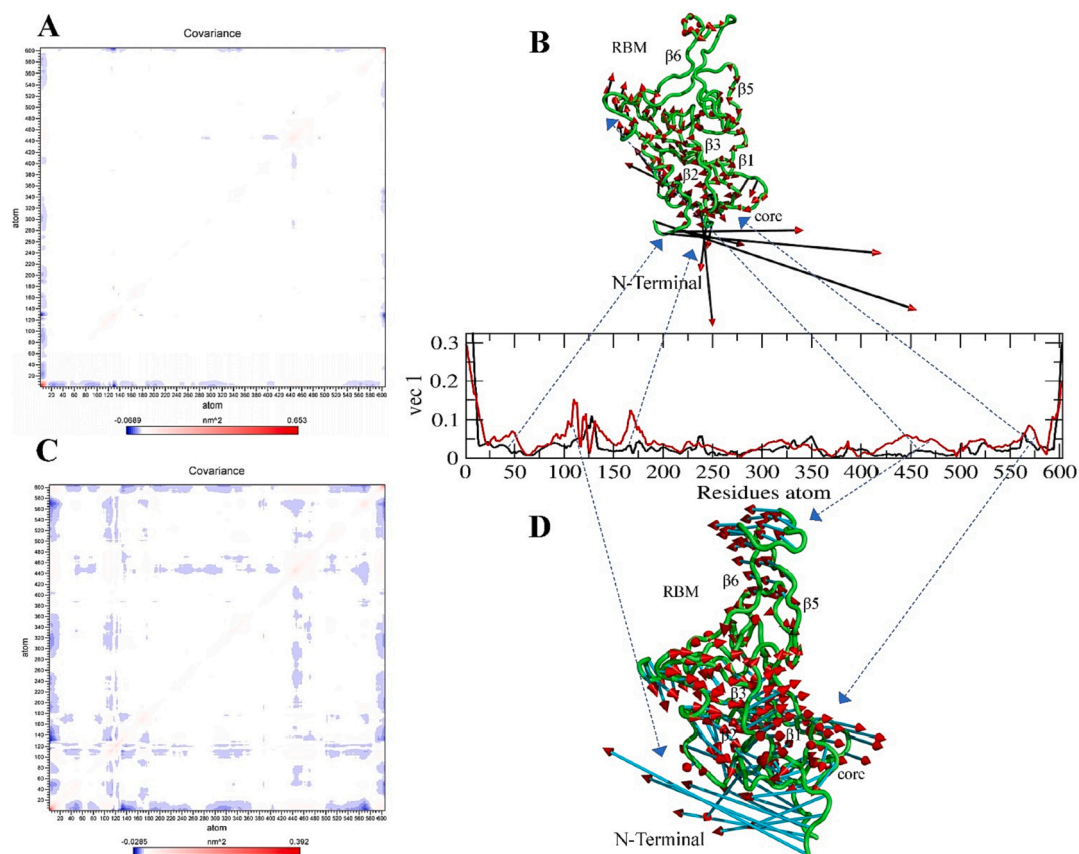


Fig. 11. Covariance and Principal Component Analysis of Omicron variant. (A, B) Total atom fluctuation and motility analyzed by covariance matrix and PCA for the apo omicron and (C, D) Ignaciomycin-omicron; (B) the black and red arrow marks indicate the atomic motion in the omicron; (D) the full cyan with red color indicates the atomic motion in the Ignaciomycin-omicron; in the covariance matrix (A, C) the red color indicates the interacting two atoms are moving together, and blue indicates atoms moving on the opposite side.

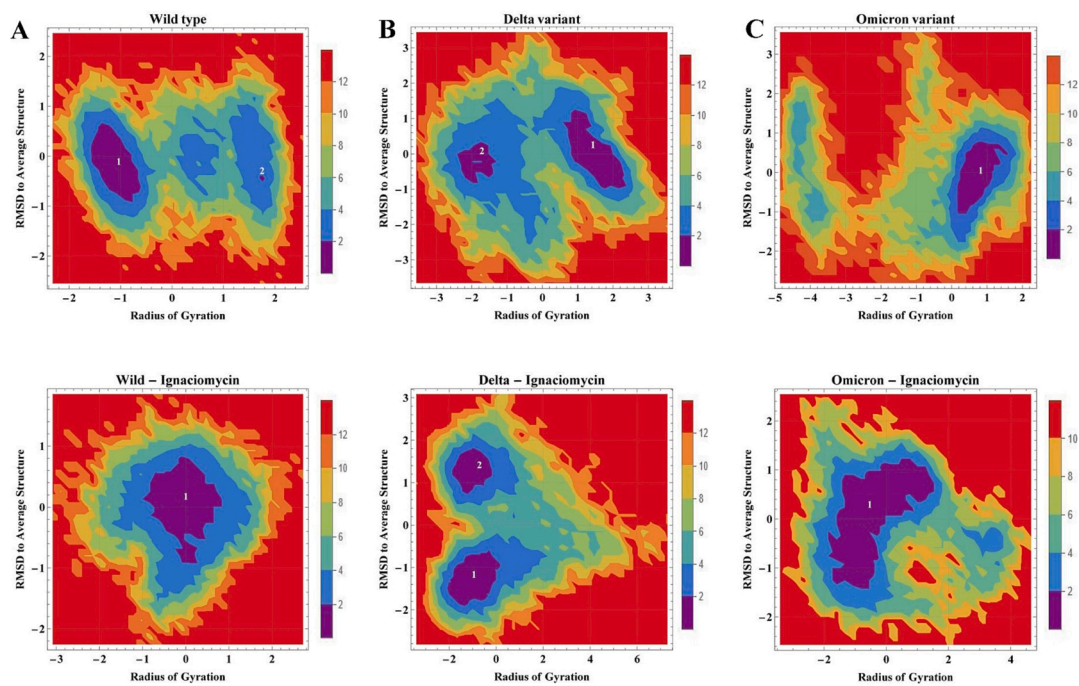


Fig. 12. Free energy landscape (FEL) plot. 2D projection of FEL of (A) wild-type, (B) Delta and (C) Omicron variant along with Ignaciomycin interaction based on the PC1 and PC2 in comparison with RMSD and Radius of gyration. The energy minima of the lowest free energy formation shown in violet and blue.

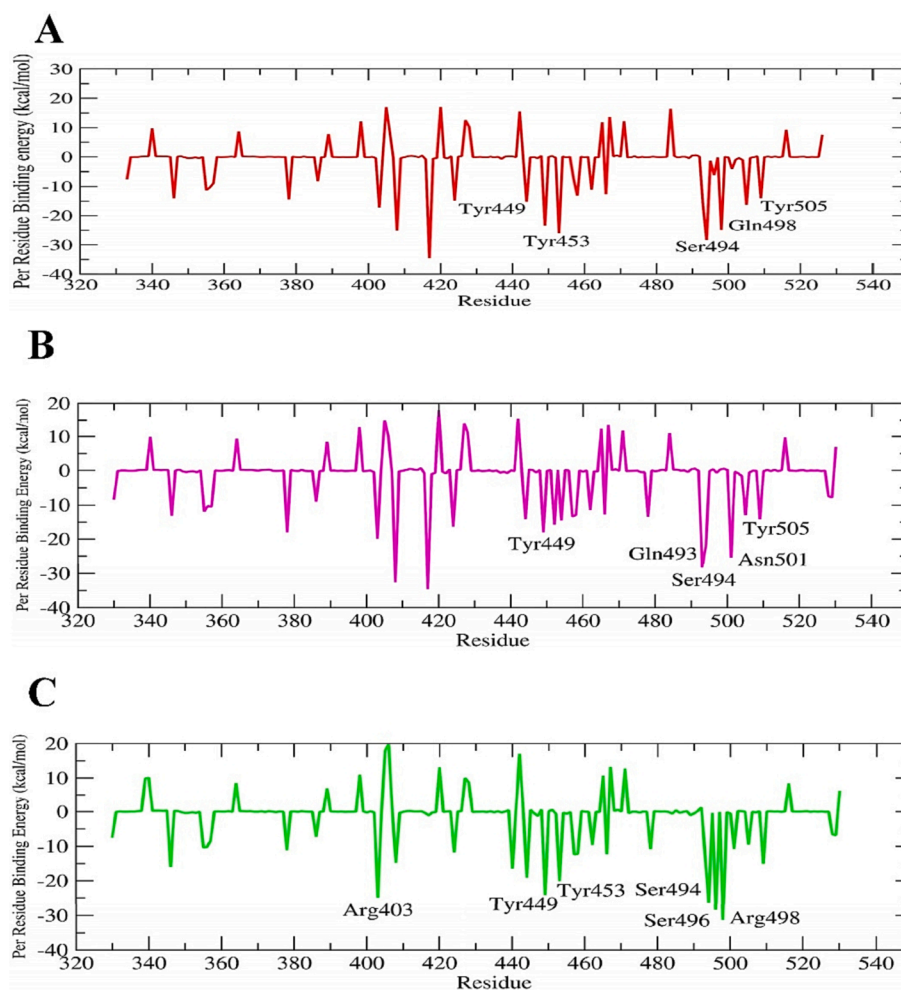


Fig. 13. The favorable per-residue energy contribution plot. Interaction energy contribution of Ignaciomycin complex with (A) wild-type, (B) delta variant, and (C) Omicron variant.

amino acids in the RBD and RBM of the SARS-CoV-2 spike glycoprotein in the wild-type, delta, and omicron variants. The binding affinities are more or less similar, and especially in the omicron variant, Ignaciomycin formed the interactions with the mutant residues Ser496, Arg498, Tyr501, His505, and also with Ser494 as in the wild-type and delta variants.

The HOMO and LUMO energies play a crucial role in detecting the reactivity of molecules used for drug design and deciding the capacities of electron-donating and attracting capabilities. The energy gap (ΔE) between HOMO and LUMO indicates the stability of the molecular surface (Houchi and Messasma, 2022b, Missioui et al., 2022). Similarly, the study of molecular ESP provides information about the electrostatic properties of molecules, such as electrophilic and nucleophilic reactions, the possibility of hydrogen bonding, and biological properties and understanding of various interactions, especially non-covalent interactions with complex biological systems (Luo et al., 2006, Spackman and Jayatilaka, 2009, Hazra et al., 2019, Singh et al., 2022). According to ESP mapping (Fig. 4B), Ignaciomycin shows electrostatic negative charges at O1 and O3 in the quinone ring, O4 of the amide, and O6, O7, and O8 of the carboxylic acid, which is involved in a strong interaction with one of the mutant residues Arg498, Ser496 and His505, which has a positive charge in Omicron. Our results are consistent with previous reports (Abian et al., 2020, Arokiyaraj et al., 2020, Oany et al., 2020, Prateeksha et al., 2021, Houchi and Messasma, 2022a, Stalin et al., 2022b).

Structural conformation and stability are important for inhibitors,

especially in infectious diseases caused by viruses, bacteria, and fungi. In the Ignaciomycin-omicron complex, the backbone RMSD equilibrated and converged throughout the simulation with moderate fluctuation around ~ 40 ns and ~ 80 ns. Even though Ignaciomycin was repositioning its structure and maintained its interaction with residues in the RBD region (Fig. 6C). H-bonds play an important role in determining the molecular stability of proteins. The secondary structure of the protein changes due to ligand interactions, and the stability of the interactions is enhanced by inter and intramolecular H-bonds (Bepari and Reza, 2021, Linani et al., 2022).

After the ~ 100 ns simulation for the wild-type, the compound Ignaciomycin maintained its stability and retained the strong conventional hydrogen bond with Tyr453, Ser494, and Tyr449 and formed a new carbon-hydrogen bond with Gln498. In addition, Ignaciomycin developed a Pi-Alkyl interaction with Tyr505. Residues Gln493, Gly496, and Asn501 were also located in the hydrophobic surface surrounding them (SI Fig. 3). Like the wild-type, Ignaciomycin in the delta and omicron variants also retained its stability. Ignaciomycin retained strong conventional hydrogen bonds in the delta variant with Gln493 and Asn501 and carbon-hydrogen bonds with Tyr449 and Ser494. In addition, Ignaciomycin maintained the Pi-Pi interaction with Tyr505 (SI Fig. 4). In the omicron variant, Ignaciomycin retained the strong conventional hydrogen bonding with Arg498, Tyr449, and Ser494 and formed a van der Waals interaction with Tyr453. In addition, Ignaciomycin formed a carbon-hydrogen bond with Ser496 and Arg403. Residues Tyr501, His505, Tyr453, and Arg493 were also located in the

hydrophobic surface region surrounded by them (SI Fig. 5).

Covariance and PCA were also performed to investigate the flexibility of atoms based on diagonalization and atomic fluctuation in the wild-type, delta, and omicron variants and their docked complexes with Ignaciomyacin. Based on the molecular dynamics simulation data, the atomic fluctuation was correlated depending on the atomic interaction between each particle in the atoms of the residues. Based on the atomic fluctuation, the degree of correlation can diverge, and especially when the particles are directly coupled with bonds, they are moved collectively, or else the particle moves in the opposite direction. These correlations between the atomic motions of the particles are related to the fluctuations in structures in the dynamic system and are related to its biological properties and functions (Fenwick et al., 2014, Chen et al., 2021).

In our study, the atom motions and the degree of collinearities for each atom pair of dynamic complexes of the Ignaciomyacin with wild-type, delta, and omicron variants were analyzed from the PCA analysis. The diagonal matrix of eigenvectors and eigenvalues summarized and confirmed the atomic fluctuations in collective motions of each particle in the spike glycoprotein and the RBD region of all complexes based on the strong interaction of Ignaciomyacin. FEL analysis also confirmed the lowest energy distribution of wild-type, delta, and omicron and the minimal energy changes after the binding of Ignaciomyacin. The ΔG -binding energy and decomposition analysis for the contribution of each residue per energy also confirmed the strong interaction of Ignaciomyacin. The overall MD simulation analysis proved the structural stability of Ignaciomyacin and the strong interaction with the RBD-ACE2 interface of SARS-CoV-2.

5. Conclusion

Docking studies revealed the strong interaction of the novel compound Ignaciomyacin with RBD of the wild-type, Delta, and Omicron. Mutations in Delta and Omicron significantly increased RBD-ACE2 binding affinity by altering their electrostatic surface and significantly increasing transmission rate and pathogenesis compared with wild-type. Ignaciomyacin exhibited strong efficiency in the mode of H-bonding interaction with the mutated sites in the RBD of Delta (TYR449, TYR453, GLN493, SER494 and ASN501) and Omicron (TYR449, ARG498, SER494, TYR501 and his505), thereby blocking the interaction between RBD and ACE2. Confirmation of the binding stability and free energy of binding of the Ignaciomyacin-RBD complex of wild-type, Delta and Omicron was also supported by ~ 100 ns dynamics simulations and MM-PBSA studies. Therefore, Ignaciomyacin could be a potential drug for treating SARS-CoV-2 mutations with resistance to existing drugs. Further experimental studies are required to confirm the mode of action of Ignaciomyacin.

Declaration of competing interest.

The author(s) declare(s) that there is no conflict of interest regarding the publication of this article.

CRedit authorship contribution statement

Antony Stalin: Conceptualization, Methodology, Software, Writing – original draft. **Pachaiyappan Saravana Kumar:** Formal analysis, Writing – review & editing. **Balakrishnan Senthamarai Kannan:** Writing – review & editing, Software, Validation. **Rajamanikam Saravanan:** Software, Validation. **Savarimuthu Ignacimuthu:** Conceptualization. **Quan Zou:** Conceptualization, Funding acquisition, Project administration.

Declaration of Competing Interest

The authors declare that they have no known competing financial interests or personal relationships that could have appeared to influence the work reported in this paper.

Acknowledgements

The work was supported by the National Natural Science Foundation of China (No. 62131004).

Appendix A. Supplementary material

Supplementary material to this article can be found online at <https://doi.org/10.1016/j.arabjc.2023.105493>.

References

- Abian, O., Ortega-Alarcon, D., Jimenez-Alesanco, A., et al., 2020. Structural stability of SARS-CoV-2 3CLpro and identification of quercetin as an inhibitor by experimental screening. *Int J Biol Macromol.* 164, 1693–1703. <https://doi.org/10.1016/j.ijbiomac.2020.07.235>.
- Abraham, M.J., Murtola, T., Schulz, R., et al., 2015. GROMACS: High performance molecular simulations through multi-level parallelism from laptops to supercomputers. *SoftwareX.* 1–2, 19–25. <https://doi.org/10.1016/j.softx.2015.06.001>.
- Akter, Y., Barua, R., Nasir Uddin, M., et al., 2022. Bioactive potentiality of secondary metabolites from endophytic bacteria against SARS-COV-2: An in-silico approach. *PLoS One.* 17, e0269962.
- Arokiyaraj, S., Stalin, A., Kannan, B.S., et al., 2020. Geranii Herba as a Potential Inhibitor of SARS-CoV-2 Main 3CL(pro), Spike RBD, and Regulation of Unfolded Protein Response: An In Silico Approach. *Antibiotics (basel).* 9 <https://doi.org/10.3390/antibiotics9120863>.
- Bajo-Morales, J., Prieto-Prieto, J.C., Herrera, L.J., et al., 2022. COVID-19 Biomarkers Recognition & Classification Using Intelligent Systems. *Current Bioinformatics.* 17, 426–439. <https://doi.org/10.2174/1574893617666220328125029>.
- Bepari, A.K., Reza, H.M., 2021. Identification of a novel inhibitor of SARS-CoV-2 3CL-PRO through virtual screening and molecular dynamics simulation. *PeerJ.* 9, e11261.
- Cao, Y., Wang, J., Jian, F., et al., 2022a. Omicron escapes the majority of existing SARS-CoV-2 neutralizing antibodies. *Nature.* 602, 657–663. <https://doi.org/10.1038/s41586-021-04385-3>.
- Cao, Y., Yisimayi, A., Jian, F., et al., 2022b. BA.2.12.1, BA.4 and BA.5 escape antibodies elicited by Omicron infection. *Nature.* 608, 593–602. <https://doi.org/10.1038/s41586-022-04980-y>.
- Chen, J., Wang, L., Wang, W., et al., 2021. Conformational transformation of switch domains in GDP/K-Ras induced by G13 mutants: An investigation through Gaussian accelerated molecular dynamics simulations and principal component analysis. *Comput Biol Med.* 135, 104639 <https://doi.org/10.1016/j.combiomed.2021.104639>.
- Chen, J., Wang, R., Gilby, N.B., et al., 2022. Omicron Variant (B.1.1.529): Infectivity, Vaccine Breakthrough, and Antibody Resistance. *J Chem Inf Model.* 62, 412–422. <https://doi.org/10.1021/acs.jcim.1c01451>.
- Cheng, S.S., Mok, C.K., Li, J.K., et al., 2022. Plaque-neutralizing antibody to BA.2.12.1, BA.4 and BA.5 in individuals with three doses of BioNTech or CoronaVac vaccines, natural infection and breakthrough infection. *J Clin Virol.* 156, 105273 <https://doi.org/10.1016/j.jcv.2022.105273>.
- Connor, J.H., McKenzie, M.O., Parks, G.D., et al., 2007. Antiviral activity and RNA polymerase degradation following Hsp90 inhibition in a range of negative strand viruses. *Virology.* 362, 109–119. <https://doi.org/10.1016/j.virol.2006.12.026>.
- Darden, T., York, D., Pedersen, L., 1993. Particle mesh Ewald: An N-log(N) method for Ewald sums in large systems. *The Journal of Chemical Physics.* 98, 10089–10092. <https://doi.org/10.1063/1.464397>.
- R.D. Dennington, T. A. K., J.M. Millam, 2016. Gauss View 6.0.16, Gaussian Inc.,
- Dong, E., Du, H., Gardner, L., 2020. An interactive web-based dashboard to track COVID-19 in real time. *The Lancet. Infectious Diseases.* 20, 533–534. [https://doi.org/10.1016/S1473-3099\(20\)30120-1](https://doi.org/10.1016/S1473-3099(20)30120-1).
- Dundas, J., Ouyang, Z., Tseng, J., et al., 2006. CASTp: computed atlas of surface topography of proteins with structural and topographical mapping of functionally annotated residues. *Nucleic Acids Res.* 34, W116–W118. <https://doi.org/10.1093/nar/gkl282>.
- Fenwick, R.B., Orellana, L., Esteban-Martin, S., et al., 2014. Correlated motions are a fundamental property of beta-sheets. *Nat Commun.* 5, 4070. <https://doi.org/10.1038/ncomms5070>.
- M. J. Frisch, G. W. T., H. B. Schlegel, G. E. Scuseria, M. A. Robb, J. R. Cheeseman, G. Scalmani, V. Barone, G. A. Petersson, H. Nakatsuji, X. Li, M. Caricato, A. Marenich, J. Bloino, B. G. Janesko, R. Gomperts, B. Mennucci, H. P. Hratchian, J. V. Ortiz, A. F. Izmaylov, J. L. Sonnenberg, D. Williams-Young, F. Ding, F. Lipparini, F. Egidi, J. Goings, B. Peng, A. Petrone, T. Henderson, D. Ranasinghe, V. G. Zakrzewski, J. Gao, N. Rega, G. Zheng, W. Liang, M. Hada, M. Ehara, K. Toyota, R. Fukuda, J. Hasegawa, M. Ishida, T. Nakajima, Y. Honda, O. Kitao, H. Nakai, T. Vreven, K. Throssell, J. A. Montgomery, Jr., J. E. Peralta, F. Ogliaro, M. Bearpark, J. J. Heyd, E. Brothers, K. N. Kudin, V. N. Staroverov, T. Keith, R. Kobayashi, J. Normand, K. Raghavachari, A. Rendell, J. C. Burant, S. S. Iyengar, J. Tomasi, M. Cossi, J. M. Millam, M. Klene, C. Adamo, R. Cammi, J. W. Ochterski, R. L. Martin, K. Morokuma, O. Farkas, J. B. Foresman, and D. J. Fox, 2016. Gaussian 09, Revision A.02. Gaussian, Inc., Wallingford CT.

- Goher, S.S., Ali, F., Amin, M., 2021. The Delta Variant Mutations in the Receptor Binding Domain of SARS-CoV-2 Show Enhanced Electrostatic Interactions with the ACE2. *Med Drug Discov.* 100114 <https://doi.org/10.1016/j.medidd.2021.100114>.
- Hazra, T., Ahmed Ullah, S., Wang, S., et al., 2019. A super-Gaussian Poisson-Boltzmann model for electrostatic free energy calculation: smooth dielectric distribution for protein cavities and in both water and vacuum states. *J Math Biol.* 79, 631–672. <https://doi.org/10.1007/s00285-019-01372-1>.
- Houchi, S., Messasma, Z., 2022a. Exploring the inhibitory potential of *Saussurea costus* and *Saussurea involucreta* phytoconstituents against the Spike glycoprotein receptor binding domain of SARS-CoV-2 Delta (B.1.617.2) variant and the main protease (M (pro)) as therapeutic candidates, using Molecular docking, DFT, and ADME/Tox studies. *J Mol Struct.* 1263, 133032 <https://doi.org/10.1016/j.molstruc.2022.133032>.
- Houchi, S., Messasma, Z., 2022b. Exploring the inhibitory potential of *Saussurea costus* and *Saussurea involucreta* phytoconstituents against the Spike glycoprotein receptor binding domain of SARS-CoV-2 Delta (B.1.617.2) variant and the main protease (Mpro) as therapeutic candidates, using Molecular docking, DFT, and ADME/Tox studies. *J Mol Struct.* 1263, 133032 <https://doi.org/10.1016/j.molstruc.2022.133032>.
- Huang, J., Rauscher, S., Nawrocki, G., et al., 2017. CHARMM36m: an improved force field for folded and intrinsically disordered proteins. *Nat Methods.* 14, 71–73. <https://doi.org/10.1038/nmeth.4067>.
- Jacob, S.G., Ali Sulaiman, M.M.B., Bennet, B., 2022. Deep Reinforcement Learning Framework for COVID Therapy: A Research Perspective. *Current Bioinformatics.* 17, 393–395. <https://doi.org/10.2174/1574893617666220329182633>.
- Kasperkiewicz, M., 2021. Covid-19, heat shock proteins, and autoimmune bullous diseases: a potential link deserving further attention. *Cell Stress Chaperones.* 26, 1–2. <https://doi.org/10.1007/s12192-020-01180-3>.
- Kousara, S., Anjuma, S.N., Jaleela, F., et al., 2017. Biomedical Significance of Tryptamine: A Review. *Journal of Pharmacovigilance.* 5 <https://doi.org/10.4172/2329-6887.1000239>.
- Kumari, R., Kumar, R., C. Open Source Drug Discovery, et al., 2014. g_mmpbsa—a GROMACS tool for high-throughput MM-PBSA calculations. *J Chem Inf Model.* 54, 1951–1962. <https://doi.org/10.1021/ci500020m>.
- Lan, J., Ge, J., Yu, J., et al., 2020. Structure of the SARS-CoV-2 spike receptor-binding domain bound to the ACE2 receptor. *Nature.* 581, 215–220. <https://doi.org/10.1038/s41586-020-2180-5>.
- Li, Y.H., Lu, Q.N., Wang, H.Q., et al., 2012. Geldanamycin, a ligand of heat shock protein 90, inhibits herpes simplex virus type 2 replication both in vitro and in vivo. *J Antibiot (tokyo).* 65, 509–512. <https://doi.org/10.1038/ja.2012.67>.
- Li, C., Tian, X., Jia, X., et al., 2021. The impact of receptor-binding domain natural mutations on antibody recognition of SARS-CoV-2. *Signal Transduct Target Ther.* 6, 132. <https://doi.org/10.1038/s41392-021-00536-0>.
- Linani, A., Benarous, K., Bou-Salah, L., et al., 2022. Exploring Structural Mechanism of COVID-19 Treatment with Glutathione as a Potential Peptide Inhibitor to the Main Protease: Molecular Dynamics Simulation and MM/PBSA Free Energy Calculations Study. *Int J Pept Res Ther.* 28, 55. <https://doi.org/10.1007/s10989-022-10365-6>.
- Lopez-Lopez, E., Naveja, J.J., Medina-Franco, J.L., 2019. DataWarrior: an evaluation of the open-source drug discovery tool. *Expert Opin Drug Discov.* 14, 335–341. <https://doi.org/10.1080/17460441.2019.1581170>.
- Luo, J., Xue, Z.Q., Liu, W.M., et al., 2006. Koopmans' theorem for large molecular systems within density functional theory. *J Phys Chem a.* 110, 12005–12009. <https://doi.org/10.1021/jp063669m>.
- Lupala, C.S., Ye, Y., Chen, H., et al., 2022. Mutations on RBD of SARS-CoV-2 Omicron variant result in stronger binding to human ACE2 receptor. *Biochem Biophys Res Commun.* 590, 34–41. <https://doi.org/10.1016/j.bbrc.2021.12.079>.
- Mahdi, M.A., Yousefi, S.R., Jasim, L.S., et al., 2022. Green synthesis of DyBa₂Fe₃O₇·988/DyFeO₃ nanocomposites using almond extract with dual eco-friendly applications: Photocatalytic and antibacterial activities. *International Journal of Hydrogen Energy.* 47, 14319–14330. <https://doi.org/10.1016/j.ijhydene.2022.02.175>.
- Missioui, M., Said, M.A., Demirtaş, G., et al., 2022. A possible potential COVID-19 drug candidate: Diethyl 2-(2-(2-(3-methyl-2-oxoquinolalin-1(2H)-yl)acetyl)hydrazono) malonate: Docking of disordered independent molecules of a novel crystal structure, HSA/DFT/XRD and cytotoxicity. *Arabian Journal of Chemistry.* 15, 103595 <https://doi.org/10.1016/j.arabjc.2021.103595>.
- Morris, G. M., R. Huey and A. J. Olson, 2008. Using AutoDock for ligand-receptor docking. *Curr Protoc Bioinformatics.* Chapter 8, Unit 8 14. <https://doi.org/10.1002/0471250953.bi0814s24>.
- Morris, G.M., Huey, R., Lindstrom, W., et al., 2009. AutoDock4 and AutoDockTools4: Automated docking with selective receptor flexibility. *J Comput Chem.* 30, 2785–2791. <https://doi.org/10.1002/jcc.21256>.
- Nikaen, G., Abbaszadeh, S., Yousefinejad, S., 2020. Application of nanomaterials in treatment, anti-infection and detection of coronaviruses. *Nanomedicine (lond).* 15, 1501–1512. <https://doi.org/10.2217/nmm-2020-0117>.
- Oany, A.R., Mia, M., Pervin, T., et al., 2020. Design of novel viral attachment inhibitors of the spike glycoprotein (S) of severe acute respiratory syndrome coronavirus-2 (SARS-CoV-2) through virtual screening and dynamics. *International Journal of Antimicrobial Agents.* 56, 106177 <https://doi.org/10.1016/j.ijantimicag.2020.106177>.
- Pachaiyappan, S.K., 2022. CCDC 2218814: Experimental Crystal Structure Determination. *CSD Communication.* <https://doi.org/10.5517/ccdc.csd.cc2dgvnd>.
- Prateeksha, G., Rana, T.S., Ashthana, A.K., et al., 2021. Screening of cryptogamic secondary metabolites as putative inhibitors of SARS-CoV-2 main protease and ribosomal binding domain of spike glycoprotein by molecular docking and molecular dynamics approaches. *J Mol Struct.* 1240, 130506 <https://doi.org/10.1016/j.molstruc.2021.130506>.
- Qu, S.J., Wang, G.F., Duan, W.H., et al., 2011. Tryptamine derivatives as novel non-nucleosidic inhibitors against hepatitis B virus. *Bioorg Med Chem.* 19, 3120–3127. <https://doi.org/10.1016/j.bmc.2011.04.004>.
- Ren, S.Y., Wang, W.B., Gao, R.D., et al., 2022. Omicron variant (B.1.1.529) of SARS-CoV-2: Mutation, infectivity, transmission, and vaccine resistance. *World J Clin Cases.* 10, 1–11. <https://doi.org/10.12998/wjcc.v10.i1.1>.
- Shang, J., Ye, G., Shi, K., et al., 2020. Structural basis of receptor recognition by SARS-CoV-2. *Nature.* 581, 221–224. <https://doi.org/10.1038/s41586-020-2179-y>.
- Singh, J.S., Khan, M.S., Uddin, S., 2022. A DFT study of vibrational spectra of 5-chlorouracil with molecular structure, HOMO-LUMO, MEPS/ESPs and thermodynamic properties. *Polym Bull (berl).* 1–29 <https://doi.org/10.1007/s00289-022-04181-7>.
- Skrzypczak, N., Pyta, K., Ruszkowski, P., et al., 2021. Anticancer activity and toxicity of new quaternary ammonium geldanamycin derivative salts and their mixtures with potentiators. *J Enzyme Inhib Med Chem.* 36, 1898–1904. <https://doi.org/10.1080/14756366.2021.1960829>.
- Spackman, M.A., Jayatilaka, D., 2009. Hirshfeld surface analysis. *CrystEngComm.* 11, 19–32. <https://doi.org/10.1039/b818330a>.
- Spackman, P.R., Turner, M.J., McKinnon, J.J., et al., 2021. CrystalExplorer: a program for Hirshfeld surface analysis, visualization and quantitative analysis of molecular crystals. *Journal of Applied Crystallography.* 54, 1006–1011. <https://doi.org/10.1107/s1600576721002910>.
- Stalin, A., Daniel Reegan, M. Rajiv Gandhi, et al., 2022. Mosquitocidal efficacy of embelin and its derivatives against *Aedes aegypti* L. and *Culex quinquefasciatus* Say. (Diptera: Culicidae) and computational analysis of acetylcholinesterase 1 (AChE1) inhibition. *Comput Biol Med.* 146, 105535. <https://doi.org/10.1016/j.combiomed.2022.105535>.
- Stalin, A., Kandhasamy, S., Kannan, B.S., et al., 2020. Synthesis of a 1,2,3-bis-triazole derivative of embelin and evaluation of its effect on high-fat diet fed-streptozotocin-induced type 2 diabetes in rats and molecular docking studies. *Bioorg Chem.* 96, 103579 <https://doi.org/10.1016/j.bioorg.2020.103579>.
- Stalin, A., Lin, D., Senthamarai Kannan, B., et al., 2022b. An in-silico approach to identify the potential hot spots in SARS-CoV-2 spike RBD to block the interaction with ACE2 receptor. *J Biomol Struct Dyn.* 40, 7408–7423. <https://doi.org/10.1080/07391102.2021.1897682>.
- Sultan, I., S. Howard and A. Tbakhi, 2020. Drug Repositioning Suggests a Role for the Heat Shock Protein 90 Inhibitor Geldanamycin in Treating COVID-19 Infection. <https://doi.org/10.21203/rs.3.rs-18714/v1>.
- Taechowisan, T., Samsawat, T., Puckdee, W., et al., 2020. Antiviral activity of geldanamycin and its derivatives against influenza virus. *Journal of Applied Pharmaceutical Science.* 10, 113–120. <https://doi.org/10.7324/japs.2020.104014>.
- Tam, N.M., Pham, M.Q., Nguyen, H.T., et al., 2021. Potential inhibitors for SARS-CoV-2 Mpro from marine compounds. *RSC Adv.* 11, 22206–22213. <https://doi.org/10.1039/d1ra03852d>.
- Tortorici, M.A., Veessler, D., 2019. Structural insights into coronavirus entry. *Adv Virus Res.* 105, 93–116. <https://doi.org/10.1016/bs.aivir.2019.08.002>.
- Van Der Spoel, D., Lindahl, E., Hess, B., et al., 2005. GROMACS: fast, flexible, and free. *J Comput Chem.* 26, 1701–1718. <https://doi.org/10.1002/jcc.20291>.
- Vanommeslaeghe, K., Hatcher, E., Acharya, C., et al., 2010. CHARMM general force field: A force field for drug-like molecules compatible with the CHARMM all-atom additive biological force fields. *J Comput Chem.* 31, 671–690. <https://doi.org/10.1002/jcc.21367>.
- Xu, F., Huang, X., Wu, H., et al., 2023. Screening compounds for treating the diabetes and COVID-19 from Miao medicine by molecular docking and bioinformatics. *Arabian Journal of Chemistry.* 16, 105001 <https://doi.org/10.1016/j.arabjc.2023.105001>.
- Yan, R., Zhang, Y., Li, Y., et al., 2020. Structural basis for the recognition of SARS-CoV-2 by full-length human ACE2. *Science.* 367, 1444–1448. <https://doi.org/10.1126/science.abb2762>.
- Yang, J., Roy, A., Zhang, Y., 2013a. BioLiP: a semi-manually curated database for biologically relevant ligand-protein interactions. *Nucleic Acids Res.* 41, D1096–D1103. <https://doi.org/10.1093/nar/gks966>.
- Yang, J., Roy, A., Zhang, Y., 2013b. Protein-ligand binding site recognition using complementary binding-specific substructure comparison and sequence profile alignment. *Bioinformatics.* 29, 2588–2595. <https://doi.org/10.1093/bioinformatics/btt447>.
- Yang, Q., Syed, A.A.S., Fahira, A., et al., 2021. Structural Analysis of the SARS-CoV-2 Omicron Variant Proteins. *Research (wash D c).* 2021, 9769586. <https://doi.org/10.34133/2021/9769586>.
- Yousefi, S.R., Alshamsi, H.A., Amiri, O., et al., 2021a. Synthesis, characterization and application of Co/Co₃O₄ nanocomposites as an effective photocatalyst for discoloration of organic dye contaminants in wastewater and antibacterial properties. *Journal of Molecular Liquids.* 337, 116405 <https://doi.org/10.1016/j.molliq.2021.116405>.
- Yousefi, S.R., Ghanbari, M., Amiri, O., et al., 2021b. Dy₂BaCuO₅/Ba₄DyCu₃O₉ S-scheme heterojunction nanocomposite with enhanced photocatalytic and antibacterial activities. *Journal of the American Ceramic Society.* 104, 2952–2965. <https://doi.org/10.1111/jace.17696>.

Zhang, Z., Cui, F., Cao, C., et al., 2021. Single-cell RNA analysis reveals the potential risk of organ-specific cell types vulnerable to SARS-CoV-2 infections. *Comput Biol Med.* 140, 105092 <https://doi.org/10.1016/j.compbiomed.2021.105092>.

Zhao, H., Lu, L., Peng, Z., et al., 2022. SARS-CoV-2 Omicron variant shows less efficient replication and fusion activity when compared with Delta variant in TMPRSS2-

expressed cells. *Emerg Microbes Infect.* 11, 277–283. <https://doi.org/10.1080/22221751.2021.2023329>.

Zulfiqar, H., Dao, F.-Y., Lv, H., et al., 2021. Identification of Potential Inhibitors Against SARS-CoV-2 Using Computational Drug Repurposing Study. *Current Bioinformatics.* 16, 1320–1327. <https://doi.org/10.2174/1574893616666210726155903>.